



HAL
open science

Multichannel fluctuating field approach to competing instabilities in interacting electronic systems

E. Linnér, A. Lichtenstein, S. Biermann, E. Stepanov

► **To cite this version:**

E. Linnér, A. Lichtenstein, S. Biermann, E. Stepanov. Multichannel fluctuating field approach to competing instabilities in interacting electronic systems. *Physical Review B*, 2023, 108 (3), pp.035143. 10.1103/PhysRevB.108.035143 . hal-04481252

HAL Id: hal-04481252

<https://hal.science/hal-04481252v1>

Submitted on 13 Nov 2024

HAL is a multi-disciplinary open access archive for the deposit and dissemination of scientific research documents, whether they are published or not. The documents may come from teaching and research institutions in France or abroad, or from public or private research centers.

L'archive ouverte pluridisciplinaire **HAL**, est destinée au dépôt et à la diffusion de documents scientifiques de niveau recherche, publiés ou non, émanant des établissements d'enseignement et de recherche français ou étrangers, des laboratoires publics ou privés.

Multi-channel fluctuating field approach to competing instabilities in interacting electronic systems

E. Linnér,¹ A. I. Lichtenstein,^{2,3,4} S. Biermann,^{1,5,6,7} and E. A. Stepanov¹

¹*CPHT, CNRS, Ecole Polytechnique, Institut Polytechnique de Paris, F-91128 Palaiseau, France*

²*I. Institute of Theoretical Physics, University of Hamburg, Jungiusstrasse 9, 20355 Hamburg, Germany*

³*European X-Ray Free-Electron Laser Facility, Holzkoppel 4, 22869 Schenefeld, Germany*

⁴*The Hamburg Centre for Ultrafast Imaging, Luruper Chaussee 149, 22761 Hamburg, Germany*

⁵*Collège de France, 11 place Marcelin Berthelot, 75005 Paris, France*

⁶*Department of Physics, Division of Mathematical Physics, Lund University, Professorgatan 1, 22363 Lund, Sweden*

⁷*European Theoretical Spectroscopy Facility, 91128 Palaiseau, France*

Systems with strong electronic Coulomb correlations often display rich phase diagrams exhibiting different ordered phases involving spin, charge, or orbital degrees of freedom. The theoretical description of the interplay of the corresponding collective fluctuations giving rise to this phenomenology remains however a tremendous challenge. Here, we introduce a multi-channel extension of the recently developed fluctuating field approach to competing collective fluctuations in correlated electron systems. The method is based on a variational optimization of a trial action that explicitly contains the order parameters of the leading fluctuation channels. It gives direct access to the free energy of the system, facilitating the distinction between stable and meta-stable phases of the system. We apply our approach to the extended Hubbard model in the weak to intermediate coupling regime where we find it to capture the interplay of competing charge density wave and antiferromagnetic fluctuations with qualitative agreement with more computationally expensive methods. The multi-channel fluctuation field approach thus offers a promising new route for a numerically cheap treatment of the interplay between collective fluctuations in large systems.

I. INTRODUCTION

A hallmark of materials with strong electronic Coulomb correlations are their typically extremely rich phase diagrams, exhibiting various kinds of ordering phenomena. These result from competing instabilities involving e.g. charge, spin, orbital or pairing fluctuations. The theoretical description of these collective phenomena remains a challenging issue of computational complexity [1, 2] as well as conceptual difficulty, e.g. the explicit breaking of symmetries [3, 4]. In this sense, the interplay of competing electronic fluctuations constitutes a roadblock to the understanding of the complex phase diagrams of a wide range of material systems. Constructing simplified methods to study interplaying collective fluctuations is thus of crucial importance.

The extended Hubbard model [5–8] provides a suitable framework for investigating the interplay between collective electronic fluctuations. The physics of this model is determined by the competition between the local U and the non-local V Coulomb interactions. A repulsive U stabilizes collective spin fluctuations [9], which may compete with charge fluctuations driven by a strong repulsive V [10, 11]. The earliest considerations of the extended Hubbard model were already implicit in the initial work of J. Hubbard in 1963 [5]. However, the first studies of the model occurred in the 1970’s, with studies of the strong [10, 12] and weak coupling limits of the half-filled one-dimensional (1D) chain [13, 14]. Together with an access to the intermediate coupling regime by early numerical exact diagonalization (ED) and lattice Monte Carlo calculations [15, 16], the phase diagram of the 1D

extended Hubbard model was predicted to be composed of regions of strong charge density wave (CDW) and antiferromagnetic (AFM) fluctuations, with a CDW-AFM transition occurring in the vicinity of $U = 2V$. The transition was later discovered to be modified in the weak coupling limit by an intermediate bond-order wave (BOW) state [17, 18].

Extensive studies have been conducted on the extended Hubbard model for elucidating the interplay between collective charge and spin fluctuations [12, 14–16, 19–28]. Considerable insight has been acquired for the extended Hubbard model on a two-dimensional square lattice at half-filling with nearest-neighbour interaction V [20–26, 29–37], which we study in the current work. It has been found that this model displays a phase diagram similar to the one-dimensional counterpart, besides the apparent lack of an intermediate BOW phase. In particular, the system reveals a checker-board CDW pattern which interplays with strong AFM fluctuations in the vicinity of a CDW-AFM transition line $U = 4V$ [20]. In a recent work [25] based on the dynamical cluster approximation (DCA) [38–40], the competition near the transition line has been shown to induce a coexistence region of charge- and spin-ordered states.

By the Mermin-Wagner theorem [41–43], magnetic ordering at finite temperatures is excluded in a broad class of one- and two-dimensional systems, including the extended Hubbard model, due to the continuous nature of the underlying symmetry. Thus, the regime of strong collective AFM fluctuations is strictly speaking not a phase. However, in our current work the “AFM phase” will refer to a slightly broader definition of short-range AFM or-

dering, which transforms to a true phase for a quasi-two-dimensional system. In contrast, the discrete symmetry of the CDW allows for a true phase transition. In addition, technically speaking, in the present work, we are performing calculations for finite systems, where long-range fluctuations are eventually cut off, so neither the AFM or CDW state are strictly speaking phases. Nevertheless, in the following, we will refer to both states as phases, since we are interested in the interplay of the competing fluctuations corresponding to these orderings. Our conclusions should thus be understood as applying either to finite systems replacing the notion of phase by "state dominated by the respective fluctuations" or to a quasi-two-dimensional system in the thermodynamic limit.

Limitations in the treatment of competing collective fluctuations arise in the currently available approaches employed for studying quantum lattice systems. Numerically exact methods, such as exact diagonalization (ED) [1] and lattice Monte Carlo [2] have studied the interplay between U and V [15, 16, 20, 21] but are restricted to small system sizes and thus cannot address long-range collective fluctuations. The same problem is also inherent in cluster extensions of the dynamical mean-field theory (DMFT) [44–49], such as, e.g., DCA [38–40]. Diagrammatic methods based on the parquet approximation [50–55] allow one to account for the interplay between charge and spin fluctuations [26] originating from the two-particle vertex functions in an unbiased and powerful fashion. These vertices are incorporated with full momentum- and frequency-dependence, and the approach is thus computationally very expensive, which severely limits its applicability. Advanced diagrammatic extensions of DMFT [56] are able to describe long-range fluctuations simultaneously in different instability channels. In the presence of the non-local interaction V this can be done within the dual boson theory [34, 36, 57–59], the dynamical vertex approximation (DGA) [60, 61], the triply irreducible local expansion (TRILEX) method [62], or the dual TRILEX (D-TRILEX) approach [27, 28, 63]. However, these fluctuations are usually treated in a ladder-like approximation, where different instability channels affect each other only indirectly via self-consistent renormalization of single- and two-particle quantities.

Current approaches to quantum lattice systems that are able to capture competing collective fluctuations are too complicated for broad usage. In this work, we develop a multi-channel generalisation of the fluctuating field (FF) approach that allows us to incorporate multiple collective fluctuation channels and their interplay in a numerically cheap way without explicitly breaking the symmetry of the model. The FF method was originally introduced for the study of spin fluctuations in the classical Ising plaquettes [64] and was further developed for single- and multi-mode treatment of collective spin fluctuations in the Hubbard model [65–67]. We employ the proposed multi-channel fluctuating field (MCFF) approach

to study the interplay between CDW and AFM fluctuations in the extended Hubbard model on a half-filled square lattice with a repulsive on-site U and nearest-neighbour V interactions. We show that the MCFF approach predicts results for the CDW and AFM phase boundaries in qualitative agreement with more elaborate numerical methods. Furthermore, it allows to model competing collective fluctuations for large system sizes near the thermodynamic limit. In addition, the method is able to distinguish between stable and meta-stable collective fluctuations. For this reason, the MCFF approach allows us to capture the true ground state of the coexistence region of CDW and AFM fluctuation that was obtained in Ref. [25] on the basis of DCA calculations.

II. MODEL

For simplicity, our considerations are limited to a single-band extended Hubbard model. However, we note that our approach can be straightforwardly generalised to more complex single- and multi-band quantum lattice systems. The Hamiltonian of the extended Hubbard model has the following form:

$$\hat{H} = -t \sum_{\langle i,j \rangle, \sigma} \hat{c}_{i\sigma}^\dagger \hat{c}_{j\sigma} + U \sum_i \hat{n}_{i\uparrow} \hat{n}_{i\downarrow} + \frac{V}{2} \sum_{\langle i,j \rangle, \sigma\sigma'} \hat{n}_{i\sigma} \hat{n}_{j\sigma'}. \quad (1)$$

In this expression, $\hat{c}_{i\sigma}^{(\dagger)}$ operators correspond to annihilation (creation) of electrons, where the subscripts denote the position i and spin projection $\sigma \in \{\uparrow, \downarrow\}$. Our system is modelled by the hopping t between nearest-neighbor sites $\langle i, j \rangle$ on a two-dimensional square lattice. The Coulomb interaction between electronic densities $\hat{n}_{i\sigma} = \hat{c}_{i\sigma}^\dagger \hat{c}_{i\sigma}$ contains the on-site U and the nearest-neighbor V components.

The extended Hubbard model (1) displays two symmetries of fundamental importance for our considerations: a continuous SU(2) symmetry associated with spin degrees of freedom and a discrete particle-hole symmetry related to charge degrees of freedom. To facilitate our later treatments, we include a sketch of the finite temperature U, V phase diagram of the extended Hubbard model on the two-dimensional square lattice in Fig. 1. Within the sketch, we denote the regime of strong CDW fluctuations (red gradient), with asymptotics of the CDW phase boundary highlighted, and the regime of strong AFM fluctuations (blue gradient). The CDW phase boundary occurs along $V = U/8 + \text{cst.}$ at weak coupling [33], which transforms to $V = U/4$ at intermediate coupling [20], followed by $V \sim U + \text{cst.}$ at strong coupling [29, 34, 36, 57, 68]. At weak coupling the AFM phase boundary starts at a critical U , which further extends to the $V = U/4$ phase boundary at intermediate coupling [25]. We restrict our consideration to the weak to intermediate coupling regime, with the strong coupling regime being outside the scope of the current work.

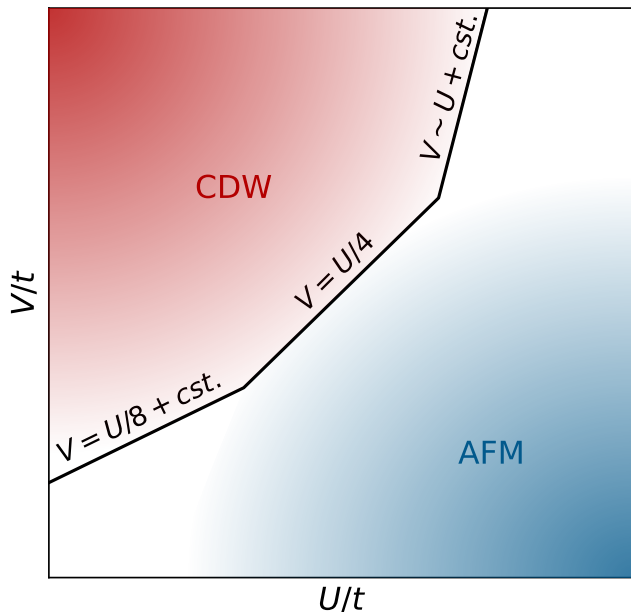


FIG. 1. Sketch of the phase diagram of the quasi-two-dimensional half-filled extended Hubbard model with repulsive interactions U and V at low but finite temperature. Beyond a critical local interactions, a regime of dominant antiferromagnetic (AFM) fluctuations is expected, while strong non-local interactions drive the system into a charge density wave (CDW) phase. At low U and V , the orderings give away for a homogeneous paramagnetic (PM) phase. The schematic phase boundaries of the CDW phase is determined by the asymptotic expressions $V = U/8 + \text{cst.}$ at weak coupling [33], $V = U/4$ at intermediate coupling [20, 21] and $V \sim U + \text{cst.}$ at strong coupling [29, 34, 36, 57, 68]. At weak to intermediate coupling, the AFM regime extrapolates from a critical U at vanishing V to the $V = U/4$ phase boundary [25].

The MCFF approach to be introduced in the next section is based on a variational principle conveniently formulated within the action formalism. Thus, it is suitable to rewrite the extended Hubbard model (1) in the form of the action:

$$S = -\frac{1}{\beta N} \sum_{\mathbf{k}, \nu, \sigma} c_{\mathbf{k}\nu\sigma}^* \mathcal{G}_{\mathbf{k}\nu}^{-1} c_{\mathbf{k}\nu\sigma} + \frac{U}{\beta N} \sum_{\mathbf{q}, \omega} \rho_{\mathbf{q}\omega\uparrow} \rho_{-\mathbf{q}, -\omega\downarrow} + \frac{1}{2\beta N} \sum_{\mathbf{q}, \omega, \sigma\sigma'} V_{\mathbf{q}} \rho_{\mathbf{q}\omega\sigma} \rho_{-\mathbf{q}, -\omega\sigma'}, \quad (2)$$

with the inverse temperature β and number of sites N . Grassmann variables $c^{(*)}$ correspond to the annihilation (creation) of electrons, where the subscripts denote the momentum \mathbf{k} and fermionic Matsubara frequency ν . The inverse of the bare (non-interacting) Green's function is defined as $\mathcal{G}_{\mathbf{k}\nu}^{-1} = i\nu + \mu - \epsilon_{\mathbf{k}}$, where μ is the chemical potential and $\epsilon_{\mathbf{k}} = -2t(\cos k_x + \cos k_y)$ is the dispersion relation for the nearest-neighbor hopping on a two-dimensional square lattice. For convenience, the interaction parts of the action (2) are written in terms of the

shifted densities $\rho_{\mathbf{q}\omega\sigma} = n_{\mathbf{q}\omega\sigma} - \langle n_{\mathbf{q}\omega\sigma} \rangle \delta_{\mathbf{q}, \mathbf{0}} \delta_{\omega, 0}$, where \mathbf{q} and ω are the momentum and bosonic Matsubara frequency indices, respectively. This choice of shift will be argued for in our later derivation. In our considerations the momentum-space representation for the non-local interaction is following $V_{\mathbf{q}} = 2V(\cos q_x + \cos q_y)$ as it is limited to only a nearest-neighbour interaction.

III. MULTI-CHANNEL FLUCTUATING FIELD METHOD

In this section we derive a multi-channel generalisation of the fluctuating field method that was originally introduced to address the fluctuations in a single (magnetic) channel [64–67]. We derive the MCFF method by utilizing a variational approach formulated in Ref. 65, which allows to incorporate the leading instabilities of the collective fluctuations.

A. Definition of trial action

We define a MC-FF trial action

$$S^* = -\frac{1}{\beta N} \sum_{\mathbf{k}, \nu, \sigma} c_{\mathbf{k}\nu\sigma}^* \mathcal{G}_{\mathbf{k}\nu}^{-1} c_{\mathbf{k}\nu\sigma} + \sum_{\mathbf{Q}, \zeta} \left[\phi_{\mathbf{Q}}^{\zeta} \rho_{-\mathbf{Q}}^{\zeta} - \frac{1}{2} \frac{\beta N}{J_{\mathbf{Q}}^{\zeta}} \phi_{\mathbf{Q}}^{\zeta} \phi_{-\mathbf{Q}}^{\zeta} \right], \quad (3)$$

that explicitly considers sets of scalar charge ($\zeta = c$) and vector spin ($\zeta = s \in \{x, y, z\}$) fields $\phi_{\mathbf{Q}}^{\zeta}$ coupled to the operators $\rho_{\mathbf{Q}}^{\zeta} = n_{\mathbf{Q}}^{\zeta} - \langle n_{\mathbf{Q}}^{\zeta} \rangle \delta_{\mathbf{Q}, \mathbf{0}}$ associated with the respective classical ($\omega = 0$) order parameters of interest. Here

$$n_{\mathbf{Q}}^{\zeta} = \frac{1}{\beta N} \sum_{\mathbf{k}, \nu, \sigma\sigma'} c_{\mathbf{k}+\mathbf{Q}, \nu\sigma}^* \sigma_{\sigma\sigma'}^{\zeta} c_{\mathbf{k}\nu\sigma'}, \quad (4)$$

where \mathbf{Q} is the ordering wave vector, σ^c is the identity and σ^s is the Pauli spin matrices. The interaction part of the trial action (3) contains a set of stiffness constants $J_{\mathbf{Q}}^{\zeta}$ that will be determined.

B. Integrating out fermionic degrees of freedom

The trial action (3) has a Gaussian form with respect to the Grassmann variables $c^{(*)}$ and classical fields ϕ^{ζ} . This allows one to obtain an effective action for either fermionic or classical degrees of freedom by analytically integrating out the other degrees of freedom. Integrating out the fermionic degrees of freedom, the effective action

for the classical fields becomes:

$$\mathcal{S}_\phi = -\text{Tr} \ln \left[\mathcal{G}_{\mathbf{k}\nu}^{-1} \delta_{\mathbf{Q},0} \delta_{\sigma,\sigma'} - \sum_{\mathbf{s}} \phi_{\mathbf{Q}}^{\mathbf{s}} \sigma_{\sigma\sigma'}^{\mathbf{s}} \right] - \frac{1}{2} \sum_{\mathbf{Q},\mathbf{s}} \frac{\beta N}{J_{\mathbf{Q}}^{\mathbf{s}}} \phi_{\mathbf{Q}}^{\mathbf{s}} \phi_{-\mathbf{Q}}^{\mathbf{s}}. \quad (5)$$

The trace is taken over the momenta \mathbf{k}, \mathbf{Q} , frequency ν , and spin σ, σ' indices. The effective action (5) depends on a small number of classical fields $\phi_{\mathbf{Q}}^{\mathbf{s}}$. For this reason, the phase diagram that captures the interplay between the different fluctuating fields can be studied by means of the free energy \mathcal{F}_ϕ corresponding to this action. Importantly, \mathcal{F}_ϕ non-perturbatively incorporates the fluctuations of the relevant order parameters $\rho_{\mathbf{Q}}^{\mathbf{s}}$ by allowing the global minimum of \mathcal{F}_ϕ to shift away from $\phi_{\mathbf{Q}}^{\mathbf{s}} = 0$.

C. Determination of the stiffness parameters via a variational principle

In order to determine $J_{\mathbf{Q}}^{\mathbf{s}}$, we use the Peierls-Feynman-Bogoliubov variational principle [69–71], as previously employed for the single-mode FF method [65]. This variational principle allows one to construct a unique and unambiguous set of $J_{\mathbf{Q}}^{\mathbf{s}}$ which minimizes the functional

$$\mathcal{F}(J_{\mathbf{Q}}^{\mathbf{s}}) = \mathcal{F}_c(J_{\mathbf{Q}}^{\mathbf{s}}) + \frac{1}{\beta N} \langle \mathcal{S} - \mathcal{S}_c \rangle_{\mathcal{S}_c} \quad (6)$$

by varying $J_{\mathbf{Q}}^{\mathbf{s}}$. Here, $\langle \dots \rangle_{\mathcal{S}_c}$ denotes the expectation value with respect to the effective fermionic action \mathcal{S}_c , corresponding to the trial action (3) with the classical fields $\phi_{\mathbf{Q}}^{\mathbf{s}}$ being integrated out:

$$\mathcal{S}_c = -\frac{1}{\beta N} \sum_{\mathbf{k},\nu,\sigma} c_{\mathbf{k}\nu\sigma}^* \mathcal{G}_{\mathbf{k}\nu}^{-1} c_{\mathbf{k}\nu\sigma} + \frac{1}{2} \sum_{\mathbf{Q},\mathbf{s}} \frac{J_{\mathbf{Q}}^{\mathbf{s}}}{\beta N} \rho_{\mathbf{Q}}^{\mathbf{s}} \rho_{-\mathbf{Q}}^{\mathbf{s}}. \quad (7)$$

In addition, we have introduced the free energy $\mathcal{F}_c(J_{\mathbf{Q}}^{\mathbf{s}}) = -\ln(\mathcal{Z}_c)/\beta N$, where \mathcal{Z}_c is the partition function of the action \mathcal{S}_c . We finally note that writing the initial (2) and the trial (3) actions in terms of $\rho^{\mathbf{s}}$ variables above allows us to keep the bare Green's function $\mathcal{G}_{\mathbf{k}\nu}$ identical in both actions, simplifying the variational treatment. In contrast, another choice of variables would necessitate a shift in the chemical potential in the trial action \mathcal{S}^* relative the extended Hubbard action \mathcal{S} .

For the evaluation of $\langle \dots \rangle_{\mathcal{S}_c}$, we explicitly rewrite the expectation value as (see Ref. 65 for details):

$$\langle \dots \rangle_{\mathcal{S}_c} = \langle \langle \dots \rangle_{\mathcal{S}_e} \rangle_{\mathcal{S}_\phi}, \quad (8)$$

where the inner expectation value is taken with respect to the fermionic part of the trial action (3):

$$\mathcal{S}_e = -\frac{1}{\beta N} \sum_{\mathbf{k},\nu,\sigma} c_{\mathbf{k}\nu\sigma}^* \mathcal{G}_{\mathbf{k}\nu}^{-1} c_{\mathbf{k}\nu\sigma} + \sum_{\mathbf{Q},\mathbf{s}} \phi_{\mathbf{Q}}^{\mathbf{s}} \rho_{-\mathbf{Q}}^{\mathbf{s}}, \quad (9)$$

which depends on the classical fields $\phi_{\mathbf{Q}}^{\mathbf{s}}$. A useful property of the inner expectation value is that Wick's theorem applies, as \mathcal{S}_e is a Gaussian action with respect to the fermions. Note that for any non-zero value of the classical field $\phi_{\mathbf{Q}}^{\mathbf{s}}$ the term $\phi_{\mathbf{Q}}^{\mathbf{s}} \rho_{-\mathbf{Q}}^{\mathbf{s}}$ in the action (9) allows for the collective fluctuations by breaking the associate symmetries in the \mathcal{S}_e sub-system. The symmetries of the full system \mathcal{S}_c are, however, retained by ultimately taking the outer expectation value $\langle \dots \rangle_{\mathcal{S}_\phi}$.

In the current work, we limit our considerations to the collective AFM and CDW fluctuations with $\mathbf{Q} = (\pi, \pi)$ wave vector that are the leading mode in the half-filled extended Hubbard model. Our choice to keep only the main \mathbf{Q} mode for each fluctuation on the grounds that the momentum-space representation for the static lattice susceptibility $X^{\mathbf{s}}(\mathbf{q}, \omega = 0)$ at the transition point between the normal and the ordered phases usually has the form of a delta-function-like Bragg peak located at the ordering vectors $X^{\mathbf{s}}(\mathbf{q}, \omega = 0) \sim \delta_{\mathbf{q},\mathbf{Q}}$ (see, e.g. Refs. [27, 28]). Thus (while a multi-mode FF has been developed to incorporate the leading and sub-leading momentum modes in [66]) we argue that considering only the leading \mathbf{Q} -mode is sufficient for predicting phase boundaries in the case of strong competing fluctuations.

Given the symmetries of the considered model, the charge and spin channels are described by two independent stiffness constants $J_{\mathbf{Q}}^{\mathbf{s}}$ and $J_{\mathbf{Q}}^{\mathbf{c}}$ that can be obtained by minimising the corresponding free energy (6) as:

$$\frac{\partial \mathcal{F}(J_{\mathbf{Q}}^{\mathbf{s}})}{\partial J_{\mathbf{Q}}^{\mathbf{s}}} = 0. \quad (10)$$

This leads to $J_{\mathbf{Q}}^{\mathbf{s}} = -U/2$ for the stiffness constant in the spin channel, in agreement with the result of the previous work [65], and to $J_{\mathbf{Q}}^{\mathbf{c}} = U/2 + V_{\mathbf{Q}}$ in the charge channel (see Appendix A for details). Importantly, the employed variational approach avoids the hidden Fierz ambiguity in the decoupling of the on-site Coulomb interaction U between the different fluctuating channels [72–74]. In this regard, it is interesting to note that the obtained values of the stiffness constants $J_{\mathbf{Q}}^{\mathbf{s}}$ correspond to the form of the bare interaction used in the diagrammatic D-TRILEX approach that resolves the Fierz ambiguity problem in a completely different way [63, 75, 76]. At this step, the effective action (5) is fully defined and can be solved numerically exactly, which allows the approach to respect the underlying symmetry of the system and in addition incorporate non-Gaussian fluctuations non-perturbatively, as will be conducted below.

D. Free energy

In this section we describe the method employed to investigate the interplay between collective CDW and AFM fluctuations in the extended Hubbard model using the developed MCFE method. The phase diagram of the system can be determined based on the free energy

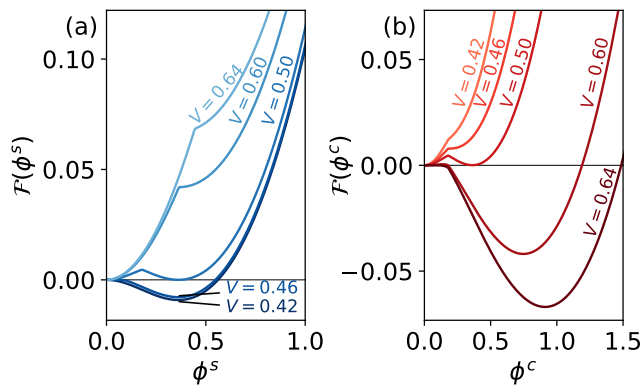


FIG. 2. Free energy $\mathcal{F}(\phi^s)$ for the spin (a) and charge (b) channels. The results are obtained for the half-filled extended Hubbard model on a square lattice at $\beta = 10/t$ and $U = 2t$ in the vicinity of the CDW-AFM transition point $V = U/4$, for a plaquette of 128×128 lattice sites. Choice of U, V are denoted as stars in Fig. 3.

\mathcal{F}_ϕ of the effective MCFF action (5), which allows us to avoid computing the more complex susceptibilities in the instability channels. In order to find the phase boundary for the CDW phase, we introduce the free energy $\mathcal{F}(\phi^c)$ for the respective classical field $\phi_{\mathbf{Q}}^c$ by integrating out the spin degrees of freedom $\phi_{\mathbf{Q}}^s$ numerically exactly:

$$\mathcal{F}(\phi^c) = -\frac{1}{\beta N} \ln \int D[\phi^s] \exp \{ -\mathcal{S}_\phi[\phi^c, \phi^s] \}. \quad (11)$$

The free energy of the classical vector spin field $\phi_{\mathbf{Q}}^s$ can be obtained in a similar way by integrating out the $\phi_{\mathbf{Q}}^c$ field. This procedure allows us to construct the free energy for a single channel that, however, fully accounts for the effect of collective fluctuations in the other channel that is integrated out. The introduced free energy has the stability requirement $J_{\mathbf{Q}}^s < 0$ that ensures that $\mathcal{F}(\phi^s)$ has a global minimum for each ϕ^s . This requirement limits the regions in which the different collective fluctuations can be incorporated within the MCFF scheme. For the considered extended Hubbard model, the stability requirement for the AFM and CDW fluctuations are $U > 0$ and $V > U/8$, respectively. With the method for constructing the free energy within the MCFF theory, we may now finally generate the U, V phase diagram for the extended Hubbard model.

IV. RESULTS

A. Phase diagram in the thermodynamic limit

We now focus on the half-filled extended Hubbard model on a square lattice with repulsive U and V interactions. The numerical MCFF investigation is based on the construction of the single-channel free energies in the CDW and AFM channel. A typical behavior of the

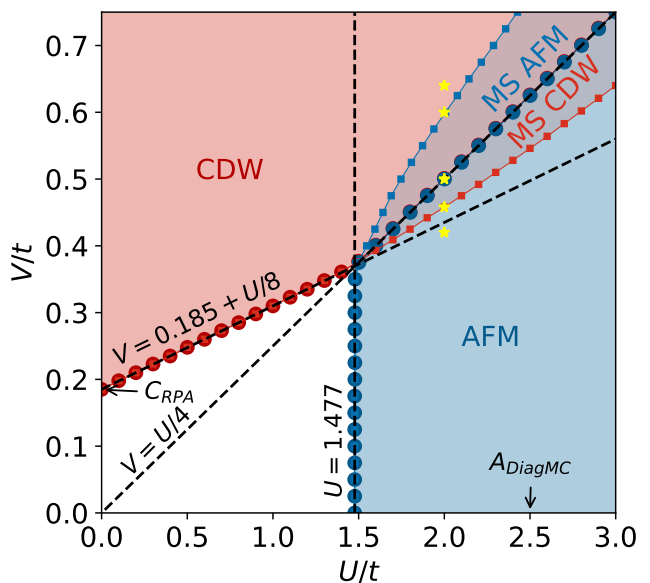


FIG. 3. Phase diagram for the half-filled extended Hubbard model with repulsive U, V interactions as predicted by the MCFF approach. The result is obtained at $\beta = 10/t$ for a plaquette of 128×128 lattice sites. Red and blue areas depict the CDW and AFM phases, respectively. The corresponding phase boundaries are shown by colored circles. Black dashed lines describe the asymptotic behavior of the phase boundaries: $V = 0.185 + U/8$ for CDW, $U = 1.477$ for AFM, and $V = U/4$ for CDW-AFM transitions. The boundaries of metastable CDW and AFM phases are illustrated by lines with small square markers. Yellow stars depict the points at which the free energies shown in Fig. 2 were calculated. For comparison, the RPA estimate C_{RPA} for the CDW boundary in the $U \rightarrow 0$, and the DiagMC estimate A_{DiagMC} for the AFM boundary in the limit of $V \rightarrow 0$, taken from Ref. [77], are included in the thermodynamic limit.

introduced single-channel free energy $\mathcal{F}(\phi^s)$ is illustrated in Fig. 2. In the normal phase, the global minimum of $\mathcal{F}(\phi^s)$ lies at $\phi^s = 0$. The formation of the ordered phase is signaled by a shift of the global minimum to a $\phi^s \neq 0$ point. In addition to the global minimum, the free energy may reveal a local minimum that indicates the presence of a metastable phase. We will discuss the appearance of the metastable phases below. Finally, we observe a non-analyticity appearing as a kink in the free energy $\mathcal{F}(\phi^s)$. It signals a change of behaviour of $\mathcal{F}(\phi^s)$ between the region in the vicinity of $\phi^s = 0$, where the fluctuations in the integrated channel are strong, and the region of $\phi^s \neq 0$, where the fluctuations in the considered channel are strong. Thus, the observed kink is inherently connected to the interplay between the collective CDW and AFM fluctuations.

We perform calculations for a plaquette of 128×128 lattice sites with periodic boundary conditions, which can be arguably considered as the thermodynamic limit, as we do not see any difference in the results compared to the 256×256 case. Fig. 3 shows the phase

diagram of the system obtained at $\beta = 10/t$. We note that the MCFF method can also be applied at much lower temperatures. The choice of β is due to convenience in the comparison to earlier works. Based on the free energy considerations discussed above, our calculations reveal three phases: a normal (white color), a CDW (red color), and an AFM (blue color) phase. We find that in the weak coupling regime $U \leq 1.447$ the CDW phase boundary follows the $V = 0.185 + U/8$ line. This result is in a perfect agreement with the perturbative estimation $V = C_{\text{RPA}} + U/8$ [33], where the constant C_{RPA} corresponds to the critical value of the non-local interaction for the CDW transition $V_{U=0}^{\text{CDW}}$ obtained for $U = 0$ using the random phase approximation (RPA). The RPA estimate is determined by the critical $V_{U=0}^{\text{CDW}}$ associate with a singularity in the RPA construction of the charge susceptibility at the (π, π) -point, or equivalently determined by a vanishing RPA dielectric function. For the considered system, $C_{\text{RPA}} = 0.1847$, which confirms that the MCFF theory correctly captures the exact $U \rightarrow 0$ limit for the CDW phase boundary. The AFM phase boundary in the weak coupling regime lies along the $U = 1.477$ line in agreement with the fluctuating local exchange (FLEX) result obtained for $V = 0$: $A_{\text{FLEX}} = U_{V=0}^{\text{AFM}} = 8C_{\text{RPA}}$. However, FLEX is known to underestimate the critical interaction for the AFM transition. For instance, in the thermodynamic limit the exact diagrammatic Monte Carlo (DiagMC) solution gives $A_{\text{DiagMC}} \simeq 2.5$ for $\beta = 10/t$ [77]. Determination of $U_{V=0}^{\text{AFM}}$ within FLEX is similar to the RPA estimate of the critical $V_{U=0}^{\text{CDW}}$, associated instead with a divergence of the FLEX construction of the spin susceptibility at the (π, π) -point. At moderate interaction strengths, if one considers fluctuations only in one channel and completely disregards the other channel, the single-channel FF method predicts the CDW and AFM phase boundary to follow exactly $V = C_{\text{RPA}} + U/8$ and $U = 8C_{\text{RPA}}$, respectively, as depicted by dashed lines in Fig. 3. The single-channel FF method thus predicts the weak interaction estimate to continue into the moderate interaction regime. If we now consider both fluctuations, the CDW and AFM phases are mutually exclusive, with the interplay leading to the system developing a CDW-AFM phase boundary at $V = U/4$ in agreement with the mean-field (RPA or GW [68]) prediction that was also confirmed by numerically exact techniques [20, 21].

Interestingly, we find that in some regions inside the CDW and AFM phases besides the global minimum the free energy $\mathcal{F}(\phi^s)$ reveals a local minimum. The appearance of the local minimum can be associated with the presence of a metastable (MS) phase. The boundaries of the metastable phases are depicted in Fig. 3 by red (MS AFM) and blue (MS CDW) lines with small square markers. Fig. 2 illustrates a particular example of the free energy behavior in the regime of strong competing CDW and AFM fluctuations. In the spin channel (Fig. 2 a)), as V is increased from deep within the AFM phase the global minimum at $\phi^s \neq 0$ in the free energy

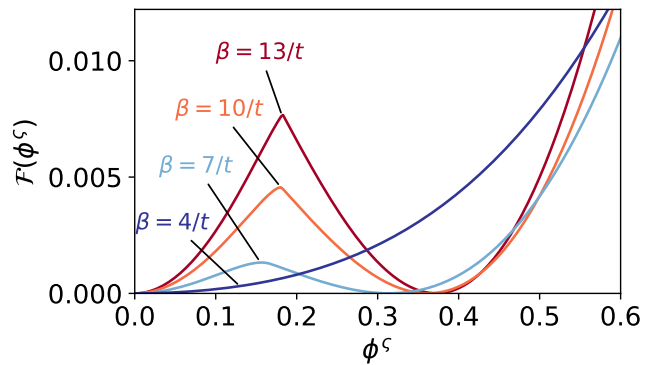


FIG. 4. Free energy $\mathcal{F}(\phi^s) = \mathcal{F}(\phi^s)$ calculated at the CDW-AFM transition point $U = 2t$, $V = 0.5t$ for a plaquette of 128×128 lattice sites, with different values of the inverse temperature β .

$\mathcal{F}(\phi^s)$ turns into a local minimum above the CDW-AFM transition point $V = U/4$, where the CDW ordering becomes dominant. The local minimum disappears at the metastable AFM phase transition point, which for $U = 2$ corresponds to $V = 0.60$. Similar results can be found for the charge channel (Fig. 2 b)): as V decreases from deep within the CDW phase the metastable CDW phase appears at the AFM-CDW transition point and vanishes at $U = 2$, $V = 0.46$.

We note that at the CDW-AFM transition the minima located at $\phi^s = 0$ and $\phi^s \neq 0$ points correspond to the same value of the free energy $\mathcal{F}(\phi^s)$. On the contrary, no metastable solution occurs in the vicinity of the phase boundaries that separate the normal phase from either the CDW or AFM phases. This result suggests that the transitions in the latter case are of second-order, while the transition between the competing CDW and AFM phases is of first-order. In addition, we find that the spin and charge channels are degenerate ($\mathcal{F}(\phi^s) = \mathcal{F}(\phi^c)$) along the CDW-AFM transition line, which indicates that the two instabilities are mutually exclusive. If these free energies were not identical at the transition point, one channel would be energetically favorable. Fig. 4 shows the behavior of the free energy $\mathcal{F}(\phi^s)$ at the CDW-AFM transition point $U = 2$, $V = 0.5$ for different temperatures. We observe that at high temperature corresponding to $\beta = 4/t$ the AFM and CDW fluctuations are suppressed, and the free energy has only one minimum at $\phi^s = 0$: the normal phase. Upon lowering the temperature the second minima develops at $\phi^s \neq 0$ and propagates to larger values of ϕ^s , corresponding to the increase of the strength of corresponding fluctuations. We also observe that the free energy barrier between the two minima increases with decreasing temperature. A larger energy barrier allows for a more stable coexistence of the two phases associated with $\phi^s = 0$ and $\phi^s \neq 0$. It should be emphasized, however, that the two channels are degenerate and that the minima at $\phi^s = 0$ and $\phi^s \neq 0$ have the same energy only at the CDW-AFM transition point.

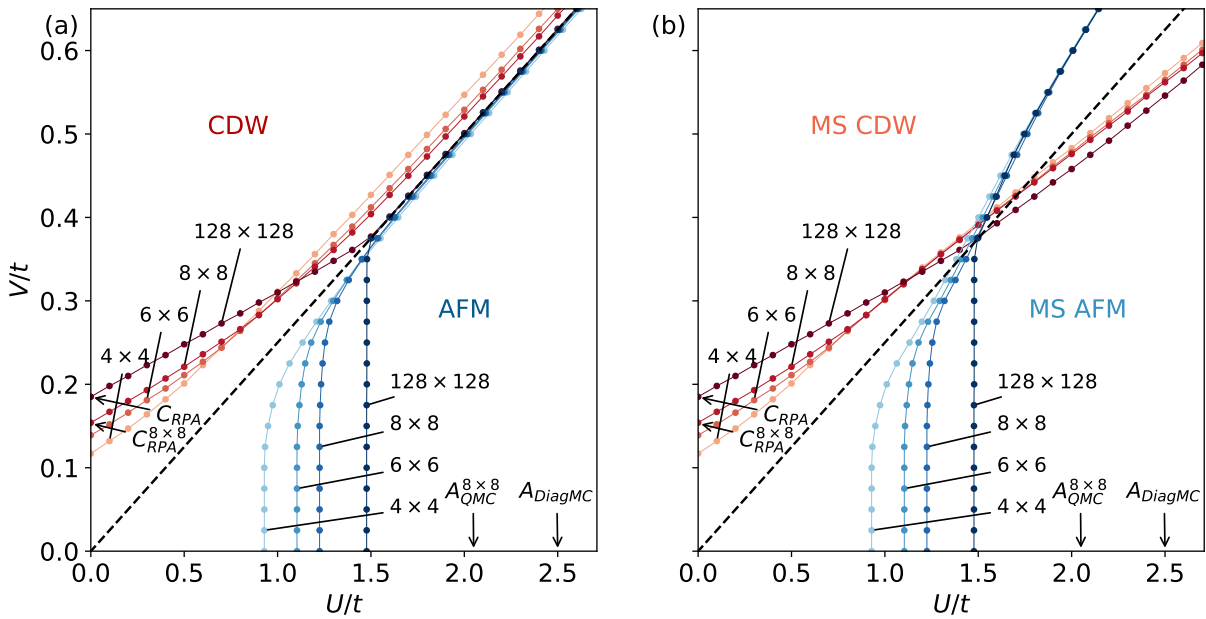


FIG. 5. Stable (a) and metastable (b) AFM (blue) and CDW (red) ordering boundaries predicted by the MCFF approach for the half-filled extended Hubbard model on 4×4 , 6×6 , 8×8 , and 128×128 plaquettes at $\beta = 10$. The dashed line specifies the mean-field estimate for the CDW-AFM phase boundary $V = U/4$. For comparison, the RPA estimates C_{RPA} and $C_{RPA}^{8 \times 8}$ for the CDW boundary in the $U \rightarrow 0$ in the thermodynamic limit and for a 8×8 plaquette, respectively, are included. In addition, the DiagMC estimate A_{DiagMC} , taken from Ref. [77], and the QMC estimate $A_{QMC}^{8 \times 8}$ for the AFM boundary in the limit of $V \rightarrow 0$ are included in the thermodynamic limit and for a 8×8 plaquette, respectively, are included.

Away from this point one of the two solutions becomes metastable, which means that one of the CDW or AFM phases always dominates. Distinguishing between stable and metastable solutions is not a trivial problem, and even the more elaborate DCA method in the regime of strong competing CDW and AFM fluctuations predicts a coexistence between these two mutually exclusive phases [25]. Thus, the ability to distinguish between the stable and the metastable phases is an advantage of the MCFF method.

B. Evolution of the phase diagram with the system size

The MCFF approach can also be applied to small systems, where its performance can be compared to the exact Monte Carlo calculations. Fig. 5 displays the stable (a) and metastable (b) ordering boundaries for AFM and CDW phases for 4×4 , 6×6 and 8×8 plaquettes, in addition to the previously considered 128×128 plaquette near the thermodynamic limit. For all system sizes the MCFF approach extrapolates the AFM and CDW ordering boundaries between weak coupling results obtained respectively on the basis of FLEX calculations and perturbative estimations, and the asymptotic behavior of the CDW-AFM phase boundary at intermediate coupling predicted by mean-field theories. A region of coexisting stable and metastable ordering is observed for all system

sizes. Phase boundaries of the coexistence region appears converged for the 128×128 plaquette, indicating its stability in the thermodynamic limit.

In order to gain insight into the performance of the MCFF approach with inclusion of collective AFM and CO fluctuations, we now perform a comparison with respect to numerically exact QMC simulations. For a 8×8 plaquette, QMC simulations give us $A_{QMC}^{8 \times 8} = 2.05 \pm 0.05$ for $\beta = 10$. By a comparison to the MCFF prediction of $U_{V=0}^{AFM} = 1.225$, we find a significant overestimation of the critical interaction U for the AFM phase boundary. This observation is consistent with our result for the 128×128 plaquette and can be related to dynamical correlation effects that are not incorporated within the approach. In contrast, the MCFF method accurately determines the CDW phase boundary at small U , with the MCFF prediction for the critical interaction $V_{U=0}^{CDW}$ coinciding with the RPA result C_{RPA} for all plaquettes sizes.

V. CONCLUSION

We have introduced a multi-channel extension of the FF approach to address interplaying collective fluctuations for correlated electronic systems, based on a variational optimization of a trial action respecting the underlying symmetries of the system. Exploiting this numerically cheap method, we are able to study competing CDW and AFM fluctuations in the half-filled ex-

tended Hubbard model of a large system size. The MCFF method predicts a repulsive $U - V$ phase diagram in qualitative agreement with more costly methods. Our approach correctly captures the $U \rightarrow 0$ limit for the CDW phase boundary, which is a non-trivial problem for computationally heavy cluster-based DMFT techniques due to the cluster size limitations. In addition, at intermediate interactions a first-order CDW-AFM transition $U = 4V$ is captured in agreement with numerically exact methods. A quantitative agreement is observed with respect to DCA simulations [25], with both approaches observing a coexistence region of collective AFM and CDW fluctuations. The coexistence regions display a strength of the MCFF approach, as it allows direct access to distinguish between the stable and metastable phases. The general nature of the MCFF theory makes it a promising

tool for studying the interplay of collective fluctuations in strongly interacting electronic systems.

ACKNOWLEDGMENTS

The authors are thankful to Alexey Rubtsov for inspiring discussions and to Maria Chatzieftheriou, Benoit Douçot, and Karyn Le Hur for useful comments. The authors also acknowledge the help of the CPHT computer support team and support from IDRIS/GENCI Orsay under project number A0130901393. The work of E.A.S was supported by the European Union's Horizon 2020 Research and Innovation programme under the Marie Skłodowska Curie grant agreement No. 839551 - 2DMAGICS.

Appendix A: Variational Principle

In this appendix we present a detailed derivation of the stiffness constant $J_{\mathbf{Q}}^{\xi}$. To this aim we apply the Peierls-Feynman-Bogoliubov variational principle that maps the initial problem (2) on the trial action (7) by minimizing the free energy $\mathcal{F}(J_{\mathbf{Q}}^{\xi})$ (6) with respect to variations in $J_{\mathbf{Q}}^{\xi}$. The free energy can be explicitly rewritten as:

$$\mathcal{F}(J_{\mathbf{Q}}^{\xi}) = \mathcal{F}_c(J_{\mathbf{Q}}^{\xi}) + \frac{1}{\beta N} \left\langle \frac{U}{\beta N} \sum_{\mathbf{q}, \omega} \rho_{\mathbf{q}\omega\uparrow} \rho_{-\mathbf{q}, -\omega\downarrow} + \frac{1}{2} \sum_{\mathbf{q}, \omega} \frac{V_{\mathbf{q}}}{\beta N} \rho_{\mathbf{q}\omega} \rho_{-\mathbf{q}, -\omega} - \sum_{\xi} \frac{1}{2} \frac{J_{\mathbf{Q}}^{\xi}}{\beta N} \rho_{\mathbf{Q}}^{\xi} \rho_{\mathbf{Q}}^{\xi} \right\rangle_{\mathcal{S}_c} \quad (\text{A1})$$

Now exploiting Eq. (8), we may rewrite the local interaction term explicitly using Wick's theorem as:

$$\begin{aligned} U \langle n_{j\tau\uparrow} n_{j\tau\downarrow} \rangle_{\mathcal{S}_c} &= U \left\langle \left\langle c_{j\tau\uparrow}^{\dagger} c_{j\tau\uparrow} c_{j\tau\downarrow}^{\dagger} c_{j\tau\downarrow} \right\rangle_{\mathcal{S}_e} \right\rangle_{\mathcal{S}_{\phi}} \\ &= U \left\langle \left\langle c_{j\tau\uparrow}^{\dagger} c_{j\tau\uparrow} \right\rangle_{\mathcal{S}_e} \left\langle c_{j\tau\downarrow}^{\dagger} c_{j\tau\downarrow} \right\rangle_{\mathcal{S}_e} - \left\langle c_{j\tau\uparrow}^{\dagger} c_{j\tau\downarrow} \right\rangle_{\mathcal{S}_e} \left\langle c_{j\tau\downarrow}^{\dagger} c_{j\tau\uparrow} \right\rangle_{\mathcal{S}_e} \right\rangle_{\mathcal{S}_{\phi}} \\ &= \frac{U}{4} \left\langle \langle n_{j\tau}^c \rangle_{\mathcal{S}_e}^2 - \langle \bar{n}_{j\tau}^s \rangle_{\mathcal{S}_e}^2 \right\rangle_{\mathcal{S}_{\phi}}, \end{aligned} \quad (\text{A2})$$

where for convenience we have employed a real-space representation for the interaction term. Rewriting the term in the Fourier basis, we arrive at:

$$\sum_{j, \tau} U \langle \rho_{j\tau\uparrow} \rho_{j\tau\downarrow} \rangle_{\mathcal{S}_c} = \frac{1}{\beta N} \sum_{\mathbf{q}, \omega} \frac{U}{4} \left\langle \left\langle \rho_{\mathbf{q}\omega}^c \right\rangle_{\mathcal{S}_e} \cdot \left\langle \rho_{-\mathbf{q}, -\omega}^c \right\rangle_{\mathcal{S}_e} - \left\langle \bar{\rho}_{\mathbf{q}\omega}^s \right\rangle_{\mathcal{S}_e} \cdot \left\langle \bar{\rho}_{-\mathbf{q}, -\omega}^s \right\rangle_{\mathcal{S}_e} \right\rangle_{\mathcal{S}_{\phi}}. \quad (\text{A3})$$

Similarly, we may rewrite the non-local interaction term approximately using Wick's theorem as:

$$\begin{aligned} \frac{1}{2} V_{ij} \langle n_{i\tau} n_{j\tau} \rangle_{\mathcal{S}_c} &= \frac{1}{2} V_{ij} \sum_{\sigma\sigma'} \left\langle \left\langle c_{i\tau\sigma}^{\dagger} c_{i\tau\sigma} c_{j\tau\sigma'}^{\dagger} c_{j\tau\sigma'} \right\rangle_{\mathcal{S}_e} \right\rangle_{\mathcal{S}_{\phi}} \\ &= \frac{1}{2} V_{ij} \sum_{\sigma\sigma'} \left\langle \left\langle c_{i\tau\sigma}^{\dagger} c_{i\tau\sigma} \right\rangle_{\mathcal{S}_e} \left\langle c_{j\tau\sigma'}^{\dagger} c_{j\tau\sigma'} \right\rangle_{\mathcal{S}_e} - \left\langle c_{i\tau\sigma}^{\dagger} c_{j\tau\sigma'} \right\rangle_{\mathcal{S}_e} \left\langle c_{j\tau\sigma'}^{\dagger} c_{i\tau\sigma} \right\rangle_{\mathcal{S}_e} \right\rangle_{\mathcal{S}_{\phi}} \\ &\approx \frac{1}{2} V_{ij} \left\langle \langle n_{i\tau}^c \rangle_{\mathcal{S}_e}^2 \right\rangle_{\mathcal{S}_{\phi}}, \end{aligned} \quad (\text{A4})$$

where $i \neq j$. Note that at the last line of this equation we have dropped the sub-leading non-local expectation values scaling as $1/N$, see Ref. [65]. Rewriting the term in the Fourier basis, we arrive at:

$$\frac{1}{2} \sum_{ij} V_{ij} \langle \rho_{i\tau} \rho_{j\tau} \rangle_{\mathcal{S}_c} \approx \frac{1}{2\beta N} \sum_{\mathbf{q}, \omega} V_{\mathbf{q}} \left\langle \left\langle \rho_{\mathbf{q}\omega}^c \right\rangle_{\mathcal{S}_e} \left\langle \rho_{-\mathbf{q}, -\omega}^c \right\rangle_{\mathcal{S}_e} \right\rangle_{\mathcal{S}_{\phi}}. \quad (\text{A5})$$

Similarly, we approximately evaluate the expectation value of the interaction in the MCFF action as:

$$\frac{1}{2} \frac{J_{\mathbf{Q}}^{\zeta}}{\beta N} \langle \rho_{\mathbf{Q}}^{\zeta 2} \rangle_{S_c} \approx \frac{1}{2} \frac{J_{\mathbf{Q}}^{\zeta}}{\beta N} \left\langle \left\langle \rho_{\mathbf{Q}}^{\zeta} \right\rangle_{S_c}^2 \right\rangle_{S_{\phi}}. \quad (\text{A6})$$

The form of the MCFF action \mathcal{S}_e (9) only allows for certain quasi-momentum modes of the local and non-local interaction terms to contribute to the free energy. Specifically, only the classical ($\omega = 0$) component with the momentum $\mathbf{q} = \mathbf{Q}$ contributes to the average of the shifted density: $\langle \rho_{\mathbf{q}\omega}^{\zeta} \rangle_{S_c} = \langle \rho_{\mathbf{Q}}^{\zeta} \rangle_{S_c}$. Thus, the free energy (A1) takes the following form:

$$\mathcal{F}(J_{\mathbf{Q}}^{\zeta}) \approx \mathcal{F}_c(J_{\mathbf{Q}}^{\zeta}) + \frac{1}{(\beta N)^2} \left(\frac{U}{4} + \frac{V_{\mathbf{Q}}}{2} - \frac{J_{\mathbf{Q}}^{\zeta}}{2} \right) \left\langle \left\langle \rho_{\mathbf{Q}}^{\zeta} \right\rangle_{S_c}^2 \right\rangle_{S_{\phi}} - \frac{1}{(\beta N)^2} \left(\frac{U}{4} + \frac{J_{\mathbf{Q}}^{\zeta}}{2} \right) \left\langle \left\langle \bar{\rho}_{\mathbf{Q}}^{\zeta} \right\rangle_{S_c}^2 \right\rangle_{S_{\phi}}. \quad (\text{A7})$$

The stiffnesses $J_{\mathbf{Q}}^{\zeta}$ may now be constructed by the proposed variational approach, by varying the free energy $\mathcal{F}(J_{\mathbf{Q}}^{\zeta})$ with respect to $J_{\mathbf{Q}}^{\zeta}$, i.e. $\partial \mathcal{F} / \partial J_{\mathbf{Q}}^{\zeta} = 0$. We thus identify $J_{\mathbf{Q}}^s = -\frac{U}{2}$ and $J_{\mathbf{Q}}^c = \frac{U}{2} + V_{\mathbf{Q}}$. This completes the determination of the stiffness constants $J_{\mathbf{Q}}^{\zeta}$.

-
- [1] C. Lanczos, “An Iteration Method for the Solution of the Eigenvalue Problem of Linear Differential and Integral Operators,” *Journal of Research of the National Bureau of Standards* **45**, 255–282 (1950).
- [2] J. E. Hirsch and R. M. Fye, “Monte Carlo Method for Magnetic Impurities in Metals,” *Phys. Rev. Lett.* **56**, 2521–2524 (1986).
- [3] M. Salmhofer, C. Honerkamp, W. Metzner, and O. Lauscher, “Renormalization Group Flows into Phases with Broken Symmetry,” *Progress of Theoretical Physics* **112**, 943–970 (2004).
- [4] P. Lykos and G. W. Pratt, “Discussion on The Hartree-Fock Approximation,” *Rev. Mod. Phys.* **35**, 496–501 (1963).
- [5] J. Hubbard, “Electron correlations in narrow energy bands,” *Proc. R. Soc. Lond. A* **276**, 238–257 (1963).
- [6] M. C. Gutzwiller, “Effect of Correlation on the Ferromagnetism of Transition Metals,” *Phys. Rev. Lett.* **10**, 159–162 (1963).
- [7] J. Kanamori, “Electron Correlation and Ferromagnetism of Transition Metals,” *Prog. Theor. Phys.* **30**, 275–289 (1963).
- [8] J. Hubbard, “Electron correlations in narrow energy bands III. An improved solution,” *Proc. R. Soc. Lond. A* **281**, 401–419 (1964).
- [9] A. B. Harris and R. V. Lange, “Single-Particle Excitations in Narrow Energy Bands,” *Phys. Rev.* **157**, 295–314 (1967).
- [10] R. A. Bari, “Effects of Short-Range Interactions on Electron-Charge Ordering and Lattice Distortions in the Localized State,” *Phys. Rev. B* **3**, 2662–2670 (1971).
- [11] S. V. Vonsovsky and M. I. Katsnelson, “Some types of instabilities in the electron energy spectrum of the polar model of the crystal. I. The maximum-polarity state,” *J. Phys. C: Solid State Phys.* **12**, 2043–2053 (1979).
- [12] V. J. Emery, “Theory of the quasi-one-dimensional electron gas with strong “on-site” interactions,” *Phys. Rev. B* **14**, 2989–2994 (1976).
- [13] J. Sólyom, “The Fermi gas model of one-dimensional conductors,” *Adv. Phys.* **28**, 201–303 (1979).
- [14] V. J. Emery, “Theory of the One-Dimensional Electron Gas,” in *Highly Conducting One-Dimensional Solids*, edited by Jozef T. Devreese, Roger P. Evrard, and Victor E. van Doren (Springer US, Boston, MA, 1979) pp. 247–303.
- [15] B. Fourcade and G. Spronken, “Real-space scaling methods applied to the one-dimensional extended Hubbard model. II. The finite-cell scaling method,” *Phys. Rev. B* **29**, 5096–5102 (1984).
- [16] J. E. Hirsch, “Charge-Density-Wave to Spin-Density-Wave Transition in the Extended Hubbard Model,” *Phys. Rev. Lett.* **53**, 2327–2330 (1984).
- [17] M. Nakamura, “Mechanism of CDW-SDW Transition in One Dimension,” *J. Phys. Soc. Jpn.* **68**, 3123–3126 (1999).
- [18] M. Nakamura, “Tricritical behavior in the extended Hubbard chains,” *Phys. Rev. B* **61**, 16377–16392 (2000).
- [19] B. Fourcade and G. Spronken, “Real-space scaling methods applied to the one-dimensional extended Hubbard model. I. The real-space renormalization-group method,” *Phys. Rev. B* **29**, 5089–5095 (1984).
- [20] Y. Zhang and J. Callaway, “Extended Hubbard model in two dimensions,” *Phys. Rev. B* **39**, 9397–9404 (1989).
- [21] J. Callaway, D. P. Chen, D. G. Kanhere, and Q. Li, “Small-cluster calculations for the simple and extended Hubbard models,” *Phys. Rev. B* **42**, 465–474 (1990).
- [22] Xin-Zhong Yan, “Theory of the extended Hubbard model at half filling,” *Phys. Rev. B* **48**, 7140–7147 (1993).
- [23] M. Aichhorn, H. G. Evertz, W. von der Linden, and M. Potthoff, “Charge ordering in extended Hubbard models: Variational cluster approach,” *Phys. Rev. B* **70**, 235107 (2004).
- [24] B. Davoudi and A.-M. S. Tremblay, “Nearest-neighbor repulsion and competing charge and spin order in the extended Hubbard model,” *Phys. Rev. B* **74**, 035113 (2006).
- [25] J. Paki, H. Terletska, S. Isakov, and E. Gull, “Charge order and antiferromagnetism in the extended Hubbard model,” *Phys. Rev. B* **99**, 245146 (2019).
- [26] P. Pudleiner, A. Kauch, K. Held, and G. Li, “Competition between antiferromagnetic and charge density wave fluctuations in the extended Hubbard model,” *Phys. Rev. B* **100**, 075108 (2019).
- [27] E. A. Stepanov, V. Harkov, M. Rösner, A. I. Lichtenstein, M. I. Katsnelson, and A. N. Rudenko, “Coexist-

- ing charge density wave and ferromagnetic instabilities in monolayer InSe,” *npj Comput. Mater.* **8**, 118 (2022).
- [28] M. Vandelli et al., to be published (2022).
- [29] T. Ayral, S. Biermann, and P. Werner, “Screening and nonlocal correlations in the extended Hubbard model from self-consistent combined *GW* and dynamical mean field theory,” *Phys. Rev. B* **87**, 125149 (2013).
- [30] H. Hafermann, E. G. C. P. van Loon, M. I. Katsnelson, A. I. Lichtenstein, and O. Parcollet, “Collective charge excitations of strongly correlated electrons, vertex corrections, and gauge invariance,” *Phys. Rev. B* **90**, 235105 (2014).
- [31] H. Terletska, T. Chen, and E. Gull, “Charge ordering and correlation effects in the extended Hubbard model,” *Phys. Rev. B* **95**, 115149 (2017).
- [32] E. G. C. P. van Loon and M. I. Katsnelson, “The extended Hubbard model with attractive interactions,” *J. Phys.: Conf. Ser.* **1136**, 012006 (2018).
- [33] A. A. Katanin, “Extended dynamical mean field theory combined with the two-particle irreducible functional renormalization-group approach as a tool to study strongly correlated systems,” *Phys. Rev. B* **99**, 115112 (2019).
- [34] M. Vandelli, V. Harkov, E. A. Stepanov, J. Gukelberger, E. Kozik, A. Rubio, and A. I. Lichtenstein, “Dual boson diagrammatic Monte Carlo approach applied to the extended Hubbard model,” *Phys. Rev. B* **102**, 195109 (2020).
- [35] H. Terletska, S. Isakov, T. Maier, and E. Gull, “Dynamical cluster approximation study of electron localization in the extended Hubbard model,” *Phys. Rev. B* **104**, 085129 (2021).
- [36] E. A. Stepanov, A. Huber, E. G. C. P. van Loon, A. I. Lichtenstein, and M. I. Katsnelson, “From local to nonlocal correlations: The Dual Boson perspective,” *Phys. Rev. B* **94**, 205110 (2016).
- [37] E. A. Stepanov, A. Huber, A. I. Lichtenstein, and M. I. Katsnelson, “Effective Ising model for correlated systems with charge ordering,” *Phys. Rev. B* **99**, 115124 (2019).
- [38] M. H. Hettler, A. N. Tahvildar-Zadeh, M. Jarrell, T. Pruschke, and H. R. Krishnamurthy, “Nonlocal dynamical correlations of strongly interacting electron systems,” *Phys. Rev. B* **58**, R7475–R7479 (1998).
- [39] M. H. Hettler, M. Mukherjee, M. Jarrell, and H. R. Krishnamurthy, “Dynamical cluster approximation: Nonlocal dynamics of correlated electron systems,” *Phys. Rev. B* **61**, 12739–12756 (2000).
- [40] K. Aryanpour, M. H. Hettler, and M. Jarrell, “Analysis of the dynamical cluster approximation for the Hubbard model,” *Phys. Rev. B* **65**, 153102 (2002).
- [41] P. C. Hohenberg, “Existence of Long-Range Order in One and Two Dimensions,” *Phys. Rev.* **158**, 383–386 (1967).
- [42] N. D. Mermin and H. Wagner, “Absence of Ferromagnetism or Antiferromagnetism in One- or Two-Dimensional Isotropic Heisenberg Models,” *Phys. Rev. Lett.* **17**, 1133–1136 (1966).
- [43] M. B. Walker and Th. W. Ruijgrok, “Absence of Magnetic Ordering in One and Two Dimensions in a Many-Band Model for Interacting Electrons in a Metal,” *Phys. Rev.* **171**, 513–515 (1968).
- [44] A. I. Lichtenstein and M. I. Katsnelson, “Antiferromagnetism and d-wave superconductivity in cuprates: A cluster dynamical mean-field theory,” *Phys. Rev. B* **62**, R9283–R9286 (2000).
- [45] G. Kotliar, S. Y. Savrasov, G. Pálsson, and G. Biroli, “Cellular Dynamical Mean Field Approach to Strongly Correlated Systems,” *Phys. Rev. Lett.* **87**, 186401 (2001).
- [46] T. Maier, M. Jarrell, T. Pruschke, and M. H. Hettler, “Quantum cluster theories,” *Rev. Mod. Phys.* **77**, 1027–1080 (2005).
- [47] A.-M. S. Tremblay, B. Kyung, and D. Sénéchal, “Pseudogap and high-temperature superconductivity from weak to strong coupling. Towards a quantitative theory (Review Article),” *Low Temp. Phys.* **32**, 424–451 (2006).
- [48] G. Kotliar, S. Y. Savrasov, K. Haule, V. S. Oudovenko, O. Parcollet, and C. A. Marianetti, “Electronic structure calculations with dynamical mean-field theory,” *Rev. Mod. Phys.* **78**, 865–951 (2006).
- [49] M. Harland, M. I. Katsnelson, and A. I. Lichtenstein, “Plaquette valence bond theory of high-temperature superconductivity,” *Phys. Rev. B* **94**, 125133 (2016).
- [50] I. T. Diatlov, V. V. Sudakov, and K. A. Ter-Martirosian, “Asymptotic meson-meson scattering theory,” *Soviet Phys. JETP* **5** (1957).
- [51] C. De Dominicis, “Variational formulations of equilibrium statistical mechanics,” *J. Math. Phys.* **3** (1962), 10.1063/1.172431.
- [52] C. De Dominicis, “Stationary entropy principle and normalization in normal and superfluid systems. I. algebraic formulation,” *J. Math. Phys.* **5** (1964), 10.1063/1.1704062.
- [53] N. E. Bickers and D. J. Scalapino, “Conserving approximations for strongly fluctuating electron systems. I. Formalism and calculational approach,” *Ann. Phys.* **193**, 206–251 (1989).
- [54] N. E. Bickers and S. R. White, “Conserving approximations for strongly fluctuating electron systems. II. Numerical results and parquet extension,” *Phys. Rev. B* **43**, 8044–8064 (1991).
- [55] N. E. Bickers, “Self-Consistent Many-Body Theory for Condensed Matter Systems,” in *Theoretical Methods for Strongly Correlated Electrons* (Springer, New York, 2004) pp. 237–296.
- [56] G. Rohringer, H. Hafermann, A. Toschi, A. A. Katanin, A. E. Antipov, M. I. Katsnelson, A. I. Lichtenstein, A. N. Rubtsov, and K. Held, “Diagrammatic routes to nonlocal correlations beyond dynamical mean field theory,” *Rev. Mod. Phys.* **90**, 025003 (2018).
- [57] E. G. C. P. van Loon, A. I. Lichtenstein, M. I. Katsnelson, O. Parcollet, and H. Hafermann, “Beyond extended dynamical mean-field theory: Dual boson approach to the two-dimensional extended Hubbard model,” *Phys. Rev. B* **90**, 235135 (2014).
- [58] E. A. Stepanov, E. G. C. P. van Loon, A. A. Katanin, A. I. Lichtenstein, M. I. Katsnelson, and A. N. Rubtsov, “Self-consistent dual boson approach to single-particle and collective excitations in correlated systems,” *Phys. Rev. B* **93**, 045107 (2016).
- [59] L. Peters, E. G. C. P. van Loon, A. N. Rubtsov, A. I. Lichtenstein, M. I. Katsnelson, and E. A. Stepanov, “Dual boson approach with instantaneous interaction,” *Phys. Rev. B* **100**, 165128 (2019).
- [60] A. Galler, P. Thunström, P. Gunacker, J. M. Tomczak, and K. Held, “Ab initio dynamical vertex approximation,” *Phys. Rev. B* **95**, 115107 (2017).
- [61] A. Galler, J. Kaufmann, P. Gunacker, M. Pickem, P. Thunström, J. M. Tomczak, and K. Held, “Towards ab initio Calculations with the Dynamical Vertex Ap-

- proximation,” *J. Phys. Soc. Jpn.* **87**, 041004 (2018).
- [62] X. Cao, T. Ayrar, Z. Zhong, O. Parcollet, D. Manske, and P. Hansmann, “Chiral d -wave superconductivity in a triangular surface lattice mediated by long-range interaction,” *Phys. Rev. B* **97**, 155145 (2018).
- [63] Matteo Vandelli, Josef Kaufmann, Mohammed El-Nabulsi, Viktor Harkov, Alexander I. Lichtenstein, and Evgeny A. Stepanov, “Multi-band D-TRILEX approach to materials with strong electronic correlations,” Preprint arXiv:2204.06426 (2022).
- [64] A. N. Rubtsov, “Fluctuating local field method probed for a description of small classical correlated lattices,” *Phys. Rev. E* **97**, 052120 (2018).
- [65] A. N. Rubtsov, E. A. Stepanov, and A. I. Lichtenstein, “Collective magnetic fluctuations in Hubbard plaquettes captured by fluctuating local field method,” *Phys. Rev. B* **102**, 224423 (2020).
- [66] Y. S. Lyakhova, E. A. Stepanov, and A. N. Rubtsov, “Fluctuating local field approach to free energy of one-dimensional molecules with strong collective electronic fluctuations,” *Phys. Rev. B* **105**, 035118 (2022).
- [67] Y. S. Lyakhova and A. N. Rubtsov, “Fluctuating local field approach to the description of lattice models in the strong coupling regime,” *J. Supercond. Nov. Magn.* **35**, 2169–2173 (2022).
- [68] T. Ayrar, S. Biermann, P. Werner, and L. Boehnke, “Influence of Fock exchange in combined many-body perturbation and dynamical mean field theory,” *Phys. Rev. B* **95**, 245130 (2017).
- [69] R. Peierls, “On a Minimum Property of the Free Energy,” *Phys. Rev.* **54**, 918–919 (1938).
- [70] N. N. Bogolyubov, “On a variational principle in the many-body problem,” *Sov. Phys. Dokl.* **3**, 292–294 (1958).
- [71] R. P. Feynman, *Statistical mechanics: A set of lectures* (Reading, Mass: Benjamin/Cummings, 1972).
- [72] J. Jaeckel and C. Wetterich, “Flow equations without mean field ambiguity,” *Phys. Rev. D* **68**, 025020 (2003).
- [73] T. Baier, E. Bick, and C. Wetterich, “Temperature dependence of antiferromagnetic order in the Hubbard model,” *Phys. Rev. B* **70**, 125111 (2004).
- [74] J. Jaeckel, “Understanding the Fierz Ambiguity of Partially Bosonized Theories,” Preprint arXiv:0205154 (2002).
- [75] E. A. Stepanov, V. Harkov, and A. I. Lichtenstein, “Consistent partial bosonization of the extended Hubbard model,” *Phys. Rev. B* **100**, 205115 (2019).
- [76] V. Harkov, M. Vandelli, S. Brener, A. I. Lichtenstein, and E. A. Stepanov, “Impact of partially bosonized collective fluctuations on electronic degrees of freedom,” *Phys. Rev. B* **103**, 245123 (2021).
- [77] F. Šimkovic, J. P. F. LeBlanc, A. J. Kim, Y. Deng, N. V. Prokof’ev, B. V. Svistunov, and E. Kozik, “Extended Crossover from a Fermi Liquid to a Quasiantiferromagnet in the Half-Filled 2D Hubbard Model,” *Phys. Rev. Lett.* **124**, 017003 (2020).